MARTIN MARIETTA ENERGY SYSTEMS LIBRARIES

3 4456 0374289 5

ornl

ORNL/TM-12219

OAK RIDGE
NATIONAL
LABORATORY

MARTIN MARIETTA

Optimization of a CO_2 Laser Thomson Scattering Alpha Particle Diagnostic

R. K. Richards
D. P. Hutchinson
C. H. Ma

OAK RIDGE NATIONAL LABORATORY
CENTRAL RESEARCH LIBRARY
CIRCULATION SECTION
4500N ROOM 175
LIBRARY LOAN COPY
DO NOT TRANSFER TO ANOTHER PERSON
If you wish someone else to see this report, send in name with report and the library will arrange a loan.

MANAGED BY
MARTIN MARIETTA ENERGY SYSTEMS, INC.
FOR THE UNITED STATES
DEPARTMENT OF ENERGY

This report has been reproduced from the best available copy.

Available to DOE and DOE contractors from the Office of Scientific and Technical Information, P.O. Box 62, Oak Ridge, TN 37831; prices available from (615) 576-8401, FTS 626-8401.

Available to the public from the National Technical Information Service, U.S. Department of Commerce, 5285 Port Royal Rd., Springfield, VA 22161.

This report was prepared as an account of work sponsored by an agency of the United States Government. Neither the United States Government nor any agency thereof, nor any of their employees, makes any warranty, express or implied, or assumes any legal liability or responsibility for the accuracy, completeness, or usefulness of any information, apparatus, product, or process disclosed, or represents that its use would not infringe privately owned rights. Reference herein to any specific commercial product, process, or service by trade name, trademark, manufacturer, or otherwise, does not necessarily constitute or imply its endorsement, recommendation, or favoring by the United States Government or any agency thereof. The views and opinions of authors expressed herein do not necessarily state or reflect those of the United States Government or any agency thereof.

ORNL/TM-12219

126
20F

Physics Division

OPTIMIZATION OF A CO_2 LASER THOMSON SCATTERING ALPHA PARTICLE DIAGNOSTIC

R. K. Richards, D. P. Hutchinson, and C. H. Ma

Date Published - January 1993

Prepared for the
Office of Fusion Energy
U.S. Department of Energy
Washington, DC 20585
Budget Activity No. AT 05 30 03 0

Prepared by the
OAK RIDGE NATIONAL LABORATORY
Oak Ridge, Tennessee 37831-6372
managed by
MARTIN MARIETTA ENERGY SYSTEMS, INC.
for the
U.S. DEPARTMENT OF ENERGY
under contract DE-AC05-84OR21400

MARTIN MARIETTA ENERGY SYSTEMS LIBRARIES

3 4456 0374289 5

Table of Contents

ABSTRACT 1

INTRODUCTION 1

DIAGNOSTIC DESCRIPTION 1

THE PLASMA 2

THEORY, MODELING, AND CALCULATIONS 3

PULSED LASER OPTIMIZATION 3

EXAMPLES 5

RECEIVER 7

DISCUSSION AND CONCLUSIONS 8

REFERENCES 8

ORNL/TM-12219

OPTIMIZATION OF A CO_2 LASER THOMSON SCATTERING ALPHA PARTICLE DIAGNOSTIC

R. K. Richards, D. P. Hutchinson, and C. H. Ma

ABSTRACT

The optimization of a CO_2 laser Thomson scattering system for measurement of the velocity distribution of fusion product alpha particles is studied. It is found that for the International Thermonuclear Experimental Reactor (ITER) plasma, the optimal system conditions are a 20-MW source laser and a receiver bandwidth of 15 GHz.

INTRODUCTION

The purpose of the CO_2 laser Thomson scattering diagnostic is to measure the velocity distribution of fusion product alpha particles in future reactors. In a D-T fusion reactor the alpha particles originate at 3.5 MeV and heat the plasma fuel as they slow down through collisional interactions. Because this plasma heating mechanism is crucial in maintaining reactor ignition, any alpha particle loss generated by plasma instabilities will degrade the reactor operation. A measurement of the alpha particle velocity distribution will allow a quantitative determination of the energy loss to the plasma due to losses of the high energy alpha particles. This report examines the optimization of the diagnostic system capable of the alpha particle velocity distribution measurement.

DIAGNOSTIC DESCRIPTION

Details of the system and its concept have been described previously;[1,2] only a brief description is, therefore, presented in the following. The system consists of a high power CO_2 source laser and a heterodyne receiver subsystem with multiple detector elements. For the plasma conditions expected in ITER, the diagnostic must operate at small angles in order to separate the alpha particle signal from the electron background. Figure 1 shows a schematic of the system. A typical scattered spectrum for this diagnostic is given in Fig. 2.

In order to have sufficient scattered signal for measurement, the source laser must be pulsed. The laser power level which optimizes the alpha particle

measurement is investigated in this report. Individual detectors are used in the receiver system to monitor the shape of the spectrum with wavelength selected by a set of local oscillators spaced over the wavelength coverage desired. The detectors are assumed to have a 50% quantum efficiency (producing a noise equivalent power of NEP = 3.75×10^{-20} W/Hz at the 10.6 micron wavelength) and a bandwidth of 2 GHz (or 1 GHz single sideband) which is within the capabilities of several detectors currently commercially available.[3]

THE PLASMA

ITER is the plasma device for which this diagnostic system is being designed. This machine is expected to operate over a range of plasma conditions and these are summarized in Table 1. The most crucial of the plasma parameters is the electron density which determines the scattering angle needed for alpha particle measurement. With electron densities around 1×10^{14} cm^{-3}, the scattering angle is typically 1°. Because the diagnostic is needed only when the alpha particle confinement is less than what was expected, the fractional alpha particle density is assumed to be 1%, not the 10% listed in Table 1. A further diagnostic requirement for this machine is the ability to spatially resolve the alpha particle velocity distribution. Because small angle scattering produces a long intersection length between the source laser and the receiver beams, good spatial resolution becomes a problem and must be considered in the optimization. It may be possible to use the tangential ports on ITER for this diagnostic; for a toroidal plasma with a major radius of 6 meters and a minor radius of approximately 2 meters, this would permit some degree of spatial resolution.

Table 1

Plasma parameter	Reference ignition	Nominal steady-state	Reference long-pulse
Density, $\langle n_e \rangle$ (10^{14} cm^{-3})	1.22	0.64	1.06
Temperature, $\langle T_e \rangle$ (keV)	10	20	11
$f_{alpha} = n_\alpha/n_e$ (%)	10	10	10

From ITER Documentation Series #33 (Vienna, 1990).

THEORY, MODELING, AND CALCULATIONS

The scattered power, P_s, within a solid angle $d\Omega$ and the frequency interval $d\omega$ is given by[4]

$$P_s = P_i\, r_0^2\, n_e\, S\, L\, d\Omega\, \frac{d\omega}{2\pi} \tag{1}$$

where P_i is the input source power, r_0 is the classical electron radius, L is the length over which the scattering is detected, and S is the spectral density function. For this analysis it is assumed that the detection of scattering is around $\phi = 0$ (i.e., in the direction parallel to B). This avoids the resonances due to effect of magnetic field when the scattering is viewed perpendicular to B, and permits the calculations to treat the particles as being nonmagnetic. The spectral density function has components from each particle species in the plasma:

$$S = S_e + S_D + S_T + S_\alpha \tag{2}$$

where S_e is the electron component, S_D the deuterium, S_T the tritium, and S_α the alpha particle; these then produce a scattered power which can be related to the plasma components:

$$P_s = P_e + P_D + P_T + P_\alpha \tag{3}$$

The components of the spectral density function are taken from ref. 1 for S_e, S_D, and S_T. For S_α the $1/v^3$ slowing down distribution proposed in ref. 5 with the corrections from ref. 6 is used.

PULSED LASER OPTIMIZATION

The optimization considered for this study is the heterodyne signal-to-noise ratio with the variables being the source laser power and pulse length. The heterodyne signal-to-noise ratio for a scattered power P_s, receiver noise NEP, receiver bandwidth B, and pulse length (integration time) τ is

$$S/N = \frac{P_s}{P_s + NEP}\sqrt{B\tau} \tag{4}$$

For a laser pulse with fixed energy (for most pulsed lasers this often means a fixed size or a fixed cost system), the scattered power is then related to the pulse length by

$$P_s \tau = constant = K \tag{5}$$

where K is determined by the energy of the laser pulse, the plasma properties, and the receiver collecting angle. The heterodyne signal-to-noise ratio as a function of P_s is then

$$S/N = \frac{P_s^{1/2}}{P_s + NEP} \sqrt{BK} \tag{6}$$

which, from solving $\frac{\delta\ S/N}{\delta\ P_s} = 0$, has a maximum at P_s = NEP. This means that for the condition of a fixed laser energy there exists an optimum laser power for maximizing the heterodyne signal-to-noise ratio. Note that this optimal laser power is not a function of the laser energy. At the optimal power (P_s = NEP), then from Eq. (4)

$$S/N|_{opt} = \frac{1}{2} \sqrt{B\tau} \tag{7}$$

By setting the desired S/N ratio equal to this optimized S/N ratio, the optimal (i.e., using the minimum energy laser pulse) signal-to-noise ratio is selected by finding the laser power for which P_s = NEP and the laser pulse length is found from Eq. (7). For example, to achieve S/N = 10 with a 2 GHz bandwidth receiver requires a laser pulse length of 0.2 μsec and S/N = 100 requires a laser pulse length of 20 μsec.

A more complicated but more realistic optimization is for conditions of measuring the alpha particle signal in the presence of an electron scattered signal and receiver noise. An example is shown in Fig. 2. A determination of the alpha particle signal at 7.5 GHz requires the measurement of the total signal at 7.5 GHz and a subtraction of the electron contribution. Fortunately, the electron scattered signal stays relatively constant and a measurement at 15 GHz can be used for this subtraction; it is assumed that the electron background is constant. With a scattered signal at 15 GHz equal to P_e, the uncertainty in the measurement (i.e., the noise level) is $\frac{P_e + NEP}{\sqrt{B\tau}}$. Similarly, with a scattered signal at 7.5 GHz being equal to $P_\alpha + P_e$ the uncertainty (noise level) in the measurement is $\frac{P_\alpha + P_e + NEP}{\sqrt{B\tau}}$. Using the difference in signals to estimate P_α produces a

conservative uncertainty equal to the sum of the noise levels, and a signal-to-noise ratio for determining the alpha particle signal as

$$S/N|_\alpha = \frac{P_\alpha}{P_\alpha + 2P_e + 2NEP}\sqrt{B\tau} \tag{8}$$

For a fixed laser energy (and noting that $P_e \propto P_\alpha \propto P_s \propto P_{laser}$) the signal-to-noise ratio can be optimized by setting $P_\alpha \tau = K$.

$$S/N|_\alpha = \frac{P_\alpha^{1/2}\sqrt{BK}}{P_\alpha + 2P_e + 2NEP} \tag{9}$$

which (from solving $\frac{\delta\ S/N|_\alpha}{\delta\ P_s} = 0$) has a maximum at $P_\alpha + 2P_e = 2$ NEP.

EXAMPLES

The measurement of the alpha particle velocity distribution requires a determination of the alpha particle scattered signal at several frequencies. If the alpha particles are lost before they are able to transfer their energy to the bulk plasma, then the shape of the scattered power spectrum changes. For example, if the alpha particles are lost as they reach half their initial energy, then the scattered spectrum in Fig. 3 would be expected which can be compared to Fig. 2 without this loss.

By measuring the ratio of scattered power at two frequencies,the energy at which alpha particles are lost can be determined as shown in Fig. 4. The flat portion at low energy loss in Fig. 4 results from the measurement at a particular frequency being sensitive to particles with velocity above some threshold, v_{crit}. The value of v_{crit} is determined by the scattering condition, $\omega/k = v_{crit}$, where k is the change in wavevector $[k = \frac{2\pi}{\lambda_l}\ 2\ \sin(\theta/2)]$ which for small angles becomes

$$v_{crit}\ (cm/sec) = 6.1 \times 10^7\ f(GHz)/\theta(deg) \tag{10}$$

It is unlikely that the alpha particles will be lost at a single energy; therefore, a measurement of the spectral shape of the scattered power would be required. The most difficult part of this measurement would be the higher frequency part of the spectrum (representing the higher energy alpha particles) because it has the

smallest signal levels. For this analysis a characteristic frequency, f_c, was selected for examining the high energy alpha particles using Eq. (10).

$$f_c\ (GHz) = \frac{\theta(deg)}{6.1 \times 10^7} \quad v_{max}(cm/sec)/\sqrt{2} \tag{11}$$

where $v_{max} = 1.32 \times 10^9$ cm/sec is the birth velocity of the alpha particles. The factor of $\sqrt{2}$ was chosen such that a measurement at f_c selects the particles with the upper half of the energy distribution.

The interaction length, L, between the pulsed laser and the receiver antenna pattern with a radius of ω_0 (called the waist) is given by

$$L = \frac{2\ \omega_0}{\sin\theta} \tag{12}$$

Using the Gaussian beam relation that the receiver beam divergency, $\Delta\theta$, is related to the waist by:

$$\Delta\theta = \frac{\lambda}{\pi\ \omega_0}, \tag{13}$$

then the interaction length for small angles ($\sin\theta = \theta$) becomes

$$L(cm) = \frac{2.22}{\theta(deg)\ \Delta\theta(deg)} \tag{14}$$

This interaction length in an alpha particle measurement is directly related to the spatial resolution of the diagnostic. At a fixed interaction length, there exists a crucial scattering angle as a function of electron density for which the scattered power from the alpha particles equals that of the electrons. This is given in Fig. 5. The optimized laser power ($P_\alpha + 2P_e = 2$ NEP) is given in Fig. 6 for this condition. Figures 5 and 6 are related through the scattering length, L and its dependence on the receiver beam divergence angle, $\Delta\theta$. As can be seen from Eq. (14), changing the scattering length while maintaining a fixed scattering angle inversely changes $\Delta\theta$. From Eq. (1) which has the scattered power proportional to $L \times \Delta\theta^2$, a change in L will then produce the inverse change in P_e or P_α. An increase in L would then require an equivalent increase in the laser power to achieve $P_\alpha + 2P_e = 2$ NEP, the condition for optimization. This result is clearly seen in Fig. 6 for the different power requirements for different scattering lengths. For electron densities $<1 \times 10^{14}$ cm^{-3} and 20 cm $< L <$ 50 cm, Fig. 6 indicates the laser power is optimized over the range 10 MW to 40 MW, i.e., the optimal laser power is 20 MW to within a factor of 2. The minimum laser power of 10 MW in Fig. 6 is set by the

convergence of θ and $\Delta\theta$. From Fig. 5, the corresponding θ at the lowest power is 0.4° at L = 20 cm; from Eq. (14), $\Delta\theta = 0.3°$. To further reduce θ would require increasing $\Delta\theta$ to where $\Delta\theta > \theta$.

A more important consideration for alpha particle measurement than achieving $P_\alpha = P_e$ is to have a sufficiently large enough signal-to-noise ratio to see changes in alpha particle distribution. The laser power optimization under conditions of a fixed signal-to-noise ratio requires further information about the laser system such as the laser pulse energy. For example, with a 100 J pulse and the alpha particle signal-to-noise ratio at 10 gives optimized scattering angle shown in Fig. 7 and the optimized laser power in Fig. 8 as functions of electron density. Under conditions of electron density $< 1 \times 10^{14}$ cm^{-3} and 20 cm < L < 50 cm from Fig. 8 again the optimized laser power is 20 MW to within a factor of 2. Again the minimum laser power is around 10 MW but in contrast to Fig. 6 the electron density in Fig. 8 is significantly lower at this minimum. The operation at lower electron density is achieved by setting a larger scattering angle for the conditions in Fig. 8 as compared to Fig. 6. Because Fig. 6 is determined by $P_\alpha = P_e$, then the requirements in Fig. 8 (i.e., $S/N|_\alpha = 10$) are met with $P_\alpha < P_e$; measurements made at $S/N|_\alpha = 10$ requires a significant correction for the electron background and it is this correction which sets the uncertainty in the determination of the alpha particle signal. Note that a 100 J laser pulse at 20 MW has a 5 μsec pulse length, giving $\sqrt{B\tau} = 100$; therefore the electron background uncertainty reduces the signal-to-noise ratio by a factor of approximately 10.

Another consideration in the selection of the source laser is the electron temperature. Variations in the electron temperature have only a slight impact in determining the crucial scattering angle which makes $P_\alpha = P_e$ (see Fig. 9). However, the optimized laser power (see Fig. 10) is strongly dependent on variations in the electron temperature. Note that the optimized laser power is inversely proportional to the electron temperature; doubling the electron temperature reduces the laser power a factor of two. Although such an electron temperature variation is proposed (see Table 1) for operation under steady-state conditions, such conditions are only likely to be met if the alpha particles are well confined and heat the bulk plasma — conditions for which this diagnostic would not be needed.

RECEIVER

The receiver configuration is based on the shape of the scattered spectrum, which results from the plasma parameters and scattering angle. For example, with a 0.5° scattering angle, as shown in Fig. 2, the shape of the spectrum could be covered with 15 GHz. If the electron density were higher, a larger scattering angle

could be used which would broaden the spectrum in proportion to the change in scattering angle. For example, with a 1° scattering angle, the spectral shape could be monitored with 30 GHz coverage. However, from Figs. 5 and 7, the measurements made with 1° scattering angle are useful only for the higher density operation. For the more typical or lower density operation, a smaller scattering angle is required which results in a reduced width of the spectrum.

DISCUSSION AND CONCLUSIONS

The optimal laser power for ITER plasma conditions is around 20 MW. This value varies with plasma condition and the need to set the scattering angle as large as possible (for the best spatial resolution), but for most conditions is between 10 and 40 MW. At the lower electron densities, the scattering angle must be kept less than 1°, which sets the spectral width for the receiver to less than 30 GHz. A limit is reached for the smallest scattering angles around 0.3° due to the large beam divergence (approaching the size of the scattering angle) required to maintain a finite spatial resolution. Near this limit (i.e., at 0.5°) the spectral width for receiver coverage is 15 GHz.

REFERENCES

1. D. P. Hutchinson, K. L. Vander Sluis, J. Sheffield, and D. J. Sigmar, Rev. Sci. Instrum. **56**, 1075 (1985).
2. R. K. Richards, C. A. Bennett, K. L. Fletcher, H. T. Hunter, and D. P. Hutchinson, Rev. Sci. Instrum. **59**, 1556 (1988).
3. C. A. Bennett, R. K. Richards, and D. P. Hutchinson, Appl. Opt. **27**, 3324 (1988).
4. J. Sheffield, *Plasma Scattering of Electromagnetic Radiation* (Academic, New York, 1975).
5. L. Vahala, G. Vahala, and D. J. Sigmar, Nucl. Fusion **26**, 51 (1986).
6. T. P. Hughes and S.R.P. Smith, Nucl. Fusion **28**, 1451 (1988).

ORNL-DWG 92M-5778

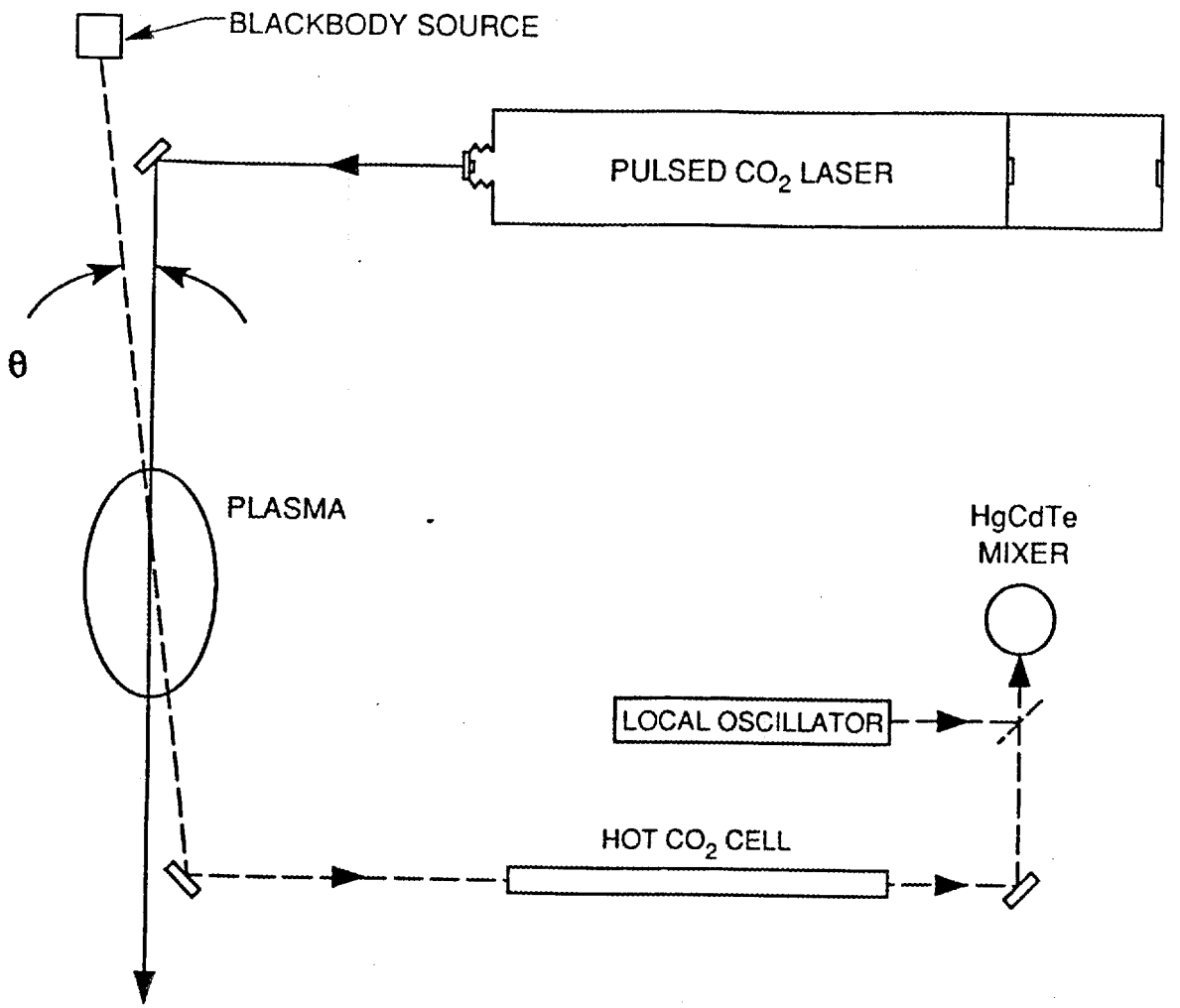

Fig. 1. Schematic of the diagnostic.

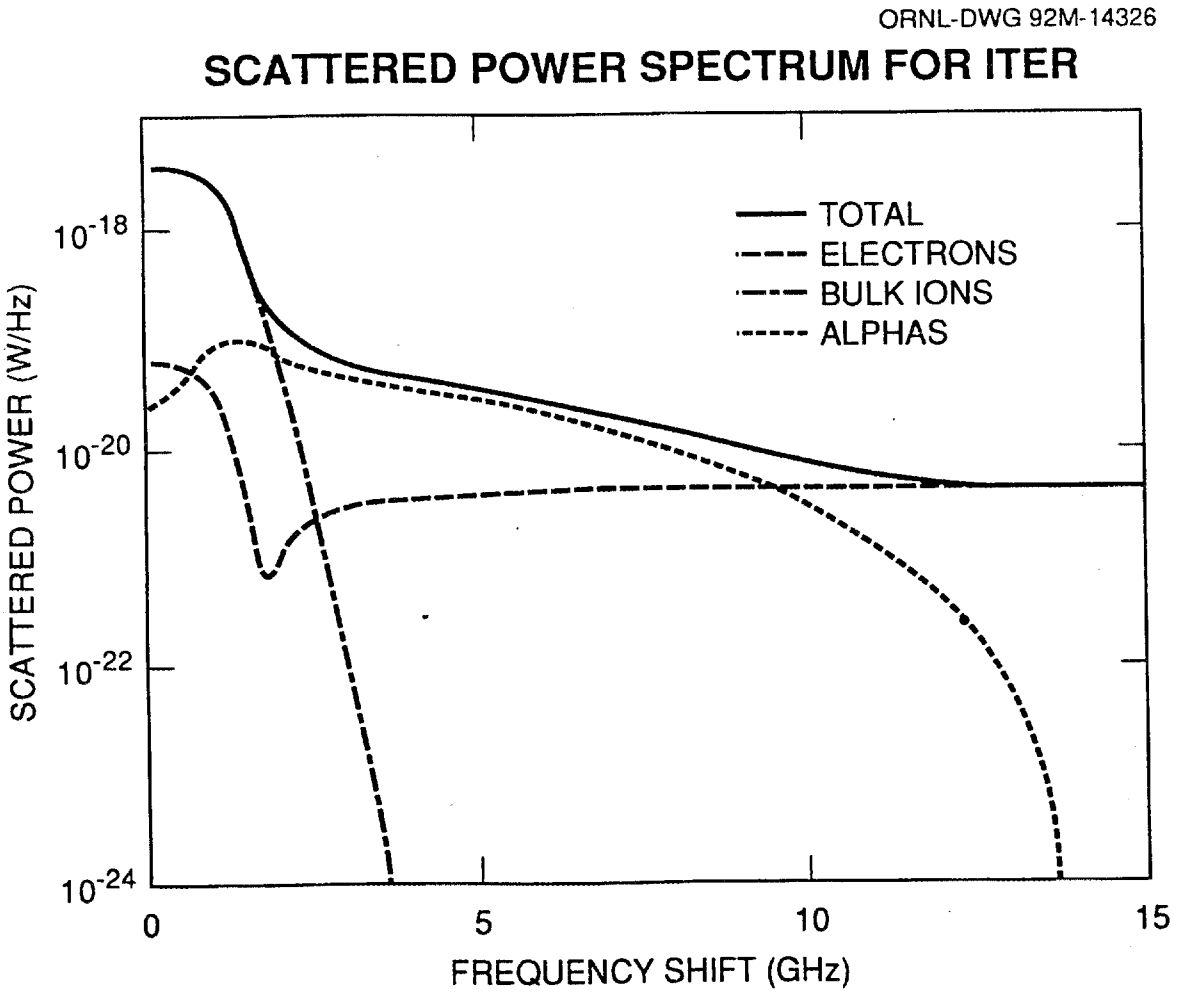

Fig. 2. Scattered power spectrum for $n_e = 1 \times 10^{14}$ cm^{-3}, $n_D = 5 \times 10^{13}$ cm^{-3}, $n_T = 2.5 \times 10^{13}$ cm^{-3}, $n_\alpha = 1 \times 10^{12}$ cm^{-3}, $T_e = T_D = T_T = 10$ keV, $P_{laser} = 10$ MW, $\theta = 0.5°$, $\Delta\theta = 0.15°$

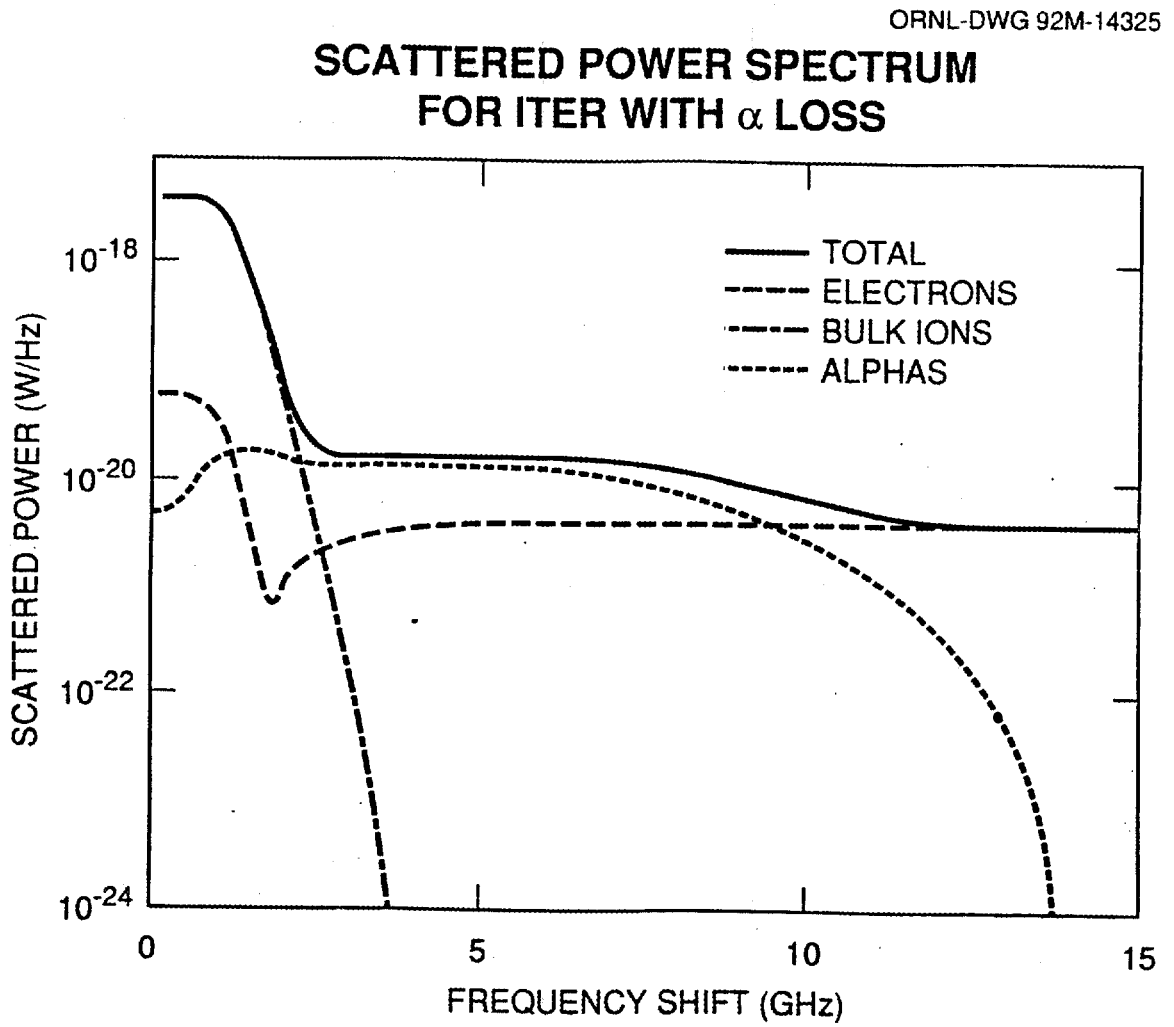

Fig. 3. Scattered power spectrum for same condition as in Fig. 2 with loss of all alpha particles with energy below 1.75 MeV.

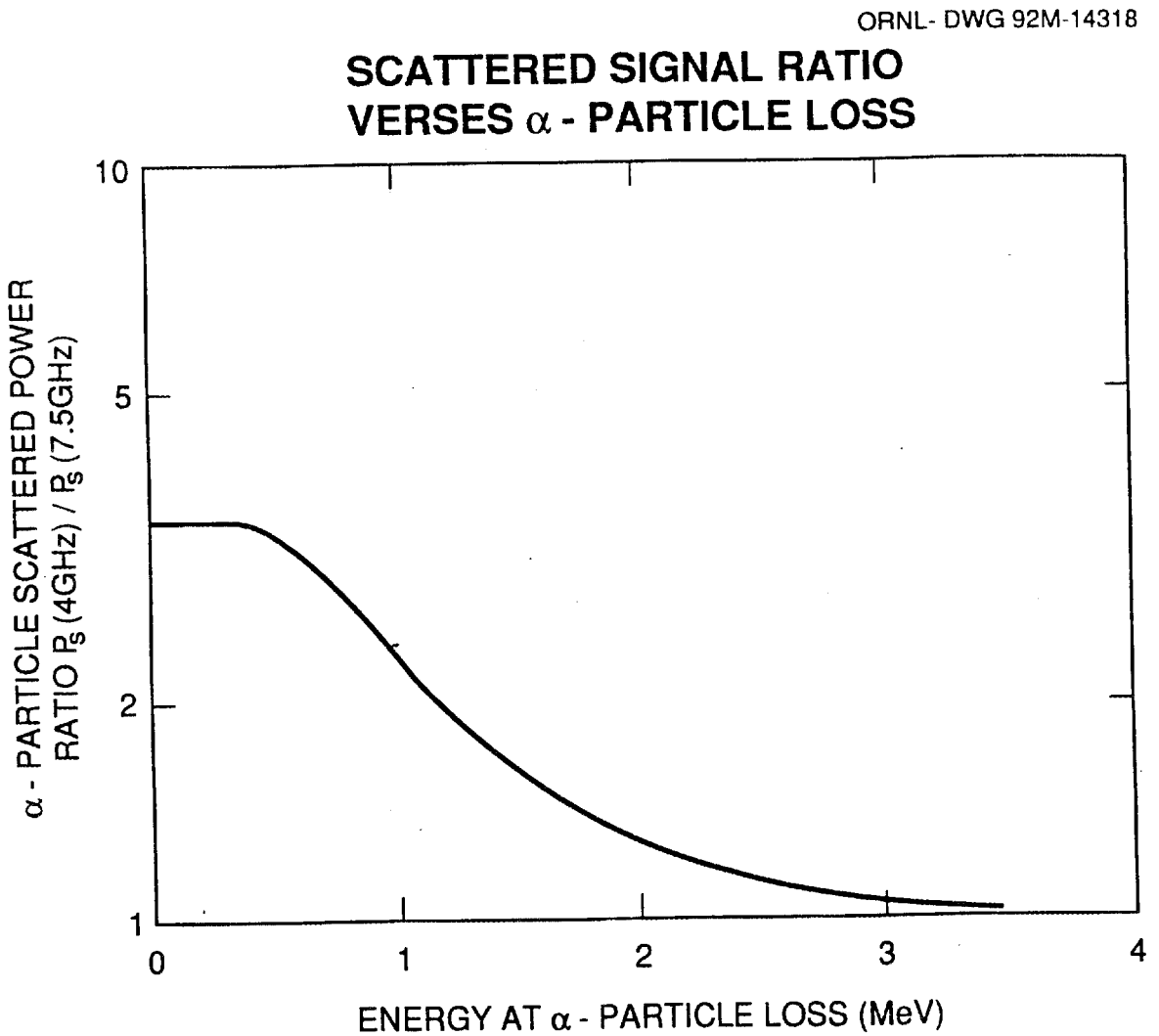

Fig. 4. Ratio of scattered powers for the alpha particles at 4 and 7.5 GHz frequency shifts versus the energy where the alpha particles are lost. The conditions are the same as in Fig. 2.

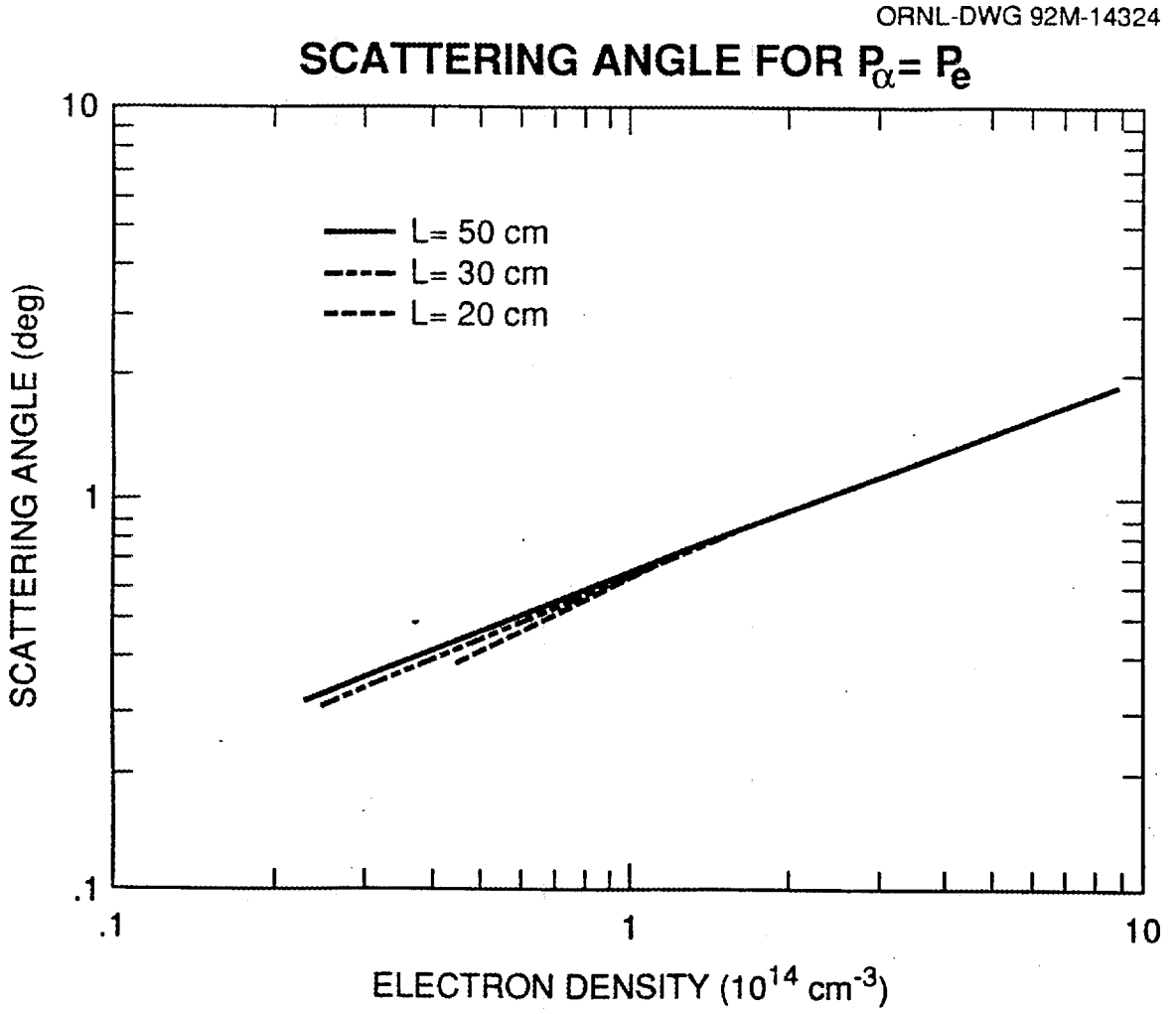

Fig. 5. The scattering angle for $P_\alpha = P_e$ versus the electron density. The alpha particle fraction is 1%, T_e = 10 keV, the receiver bandwidth is 2 GHz, and the central frequency for the receiver is set by Eq. (11). The three curves are for scattering lengths of 20, 30, and 50 cm.

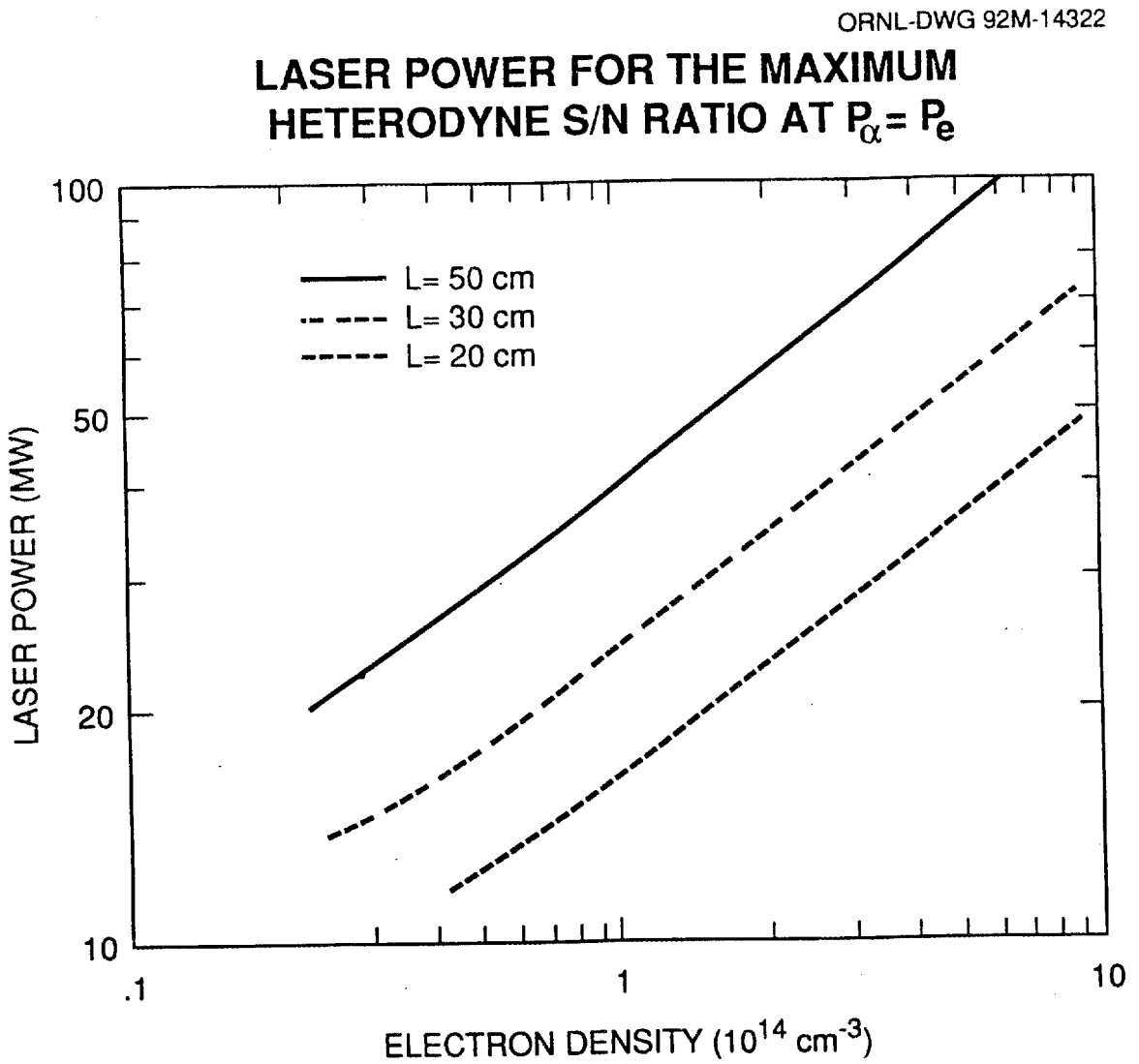

Fig. 6. The laser power which optimizes the signal-to-noise ratio versus the electron density for the conditions given in Fig. 5.

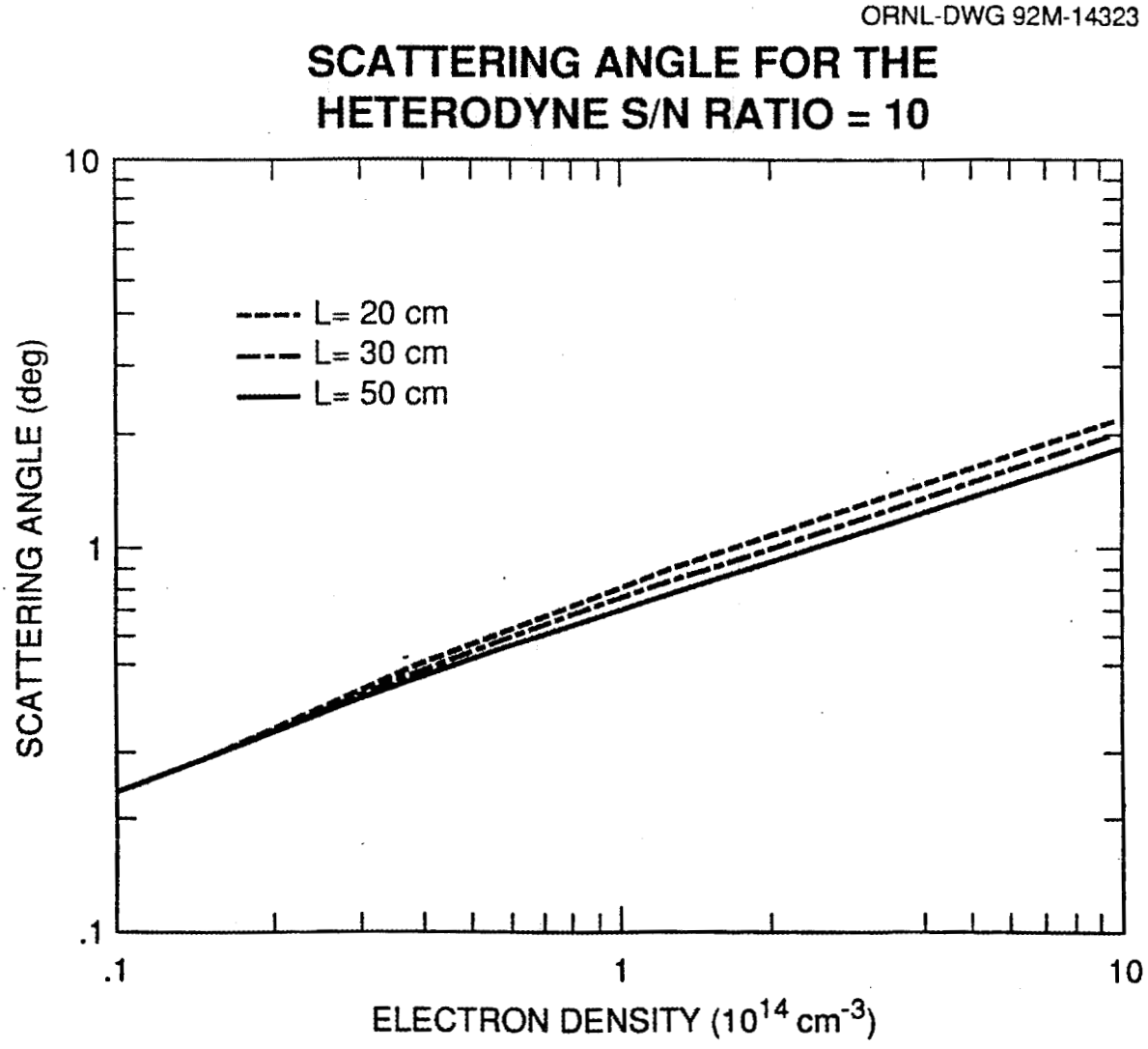

Fig. 7. The scattering angle for a signal-to-noise ratio of 10 versus the electron density for the same conditions in Fig. 5 and a laser energy of 100 Joules.

ORNL- DWG 92M-14321

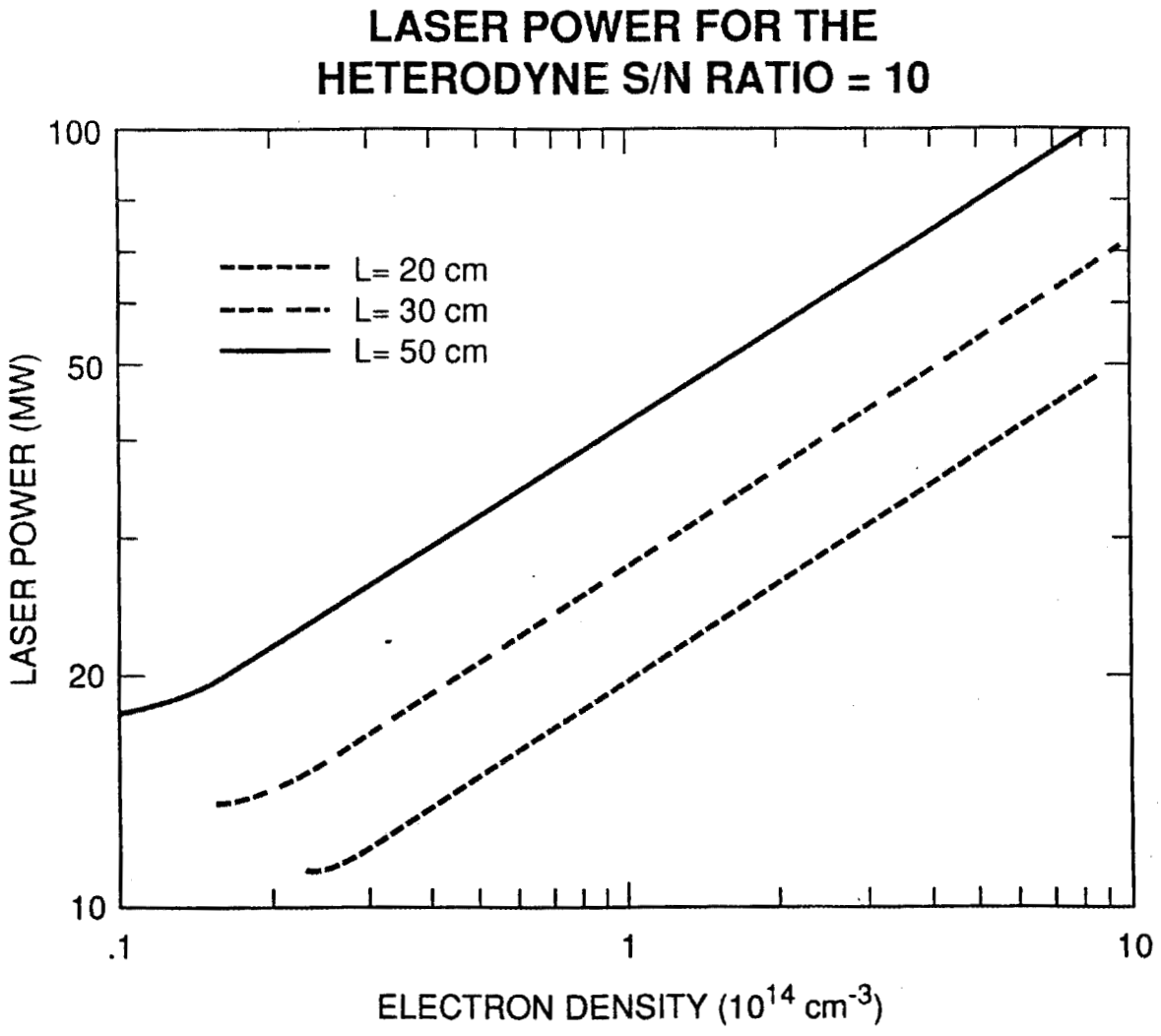

Fig. 8. The laser power which optimizes the signal-to-noise ratio for the conditions given in Fig. 7.

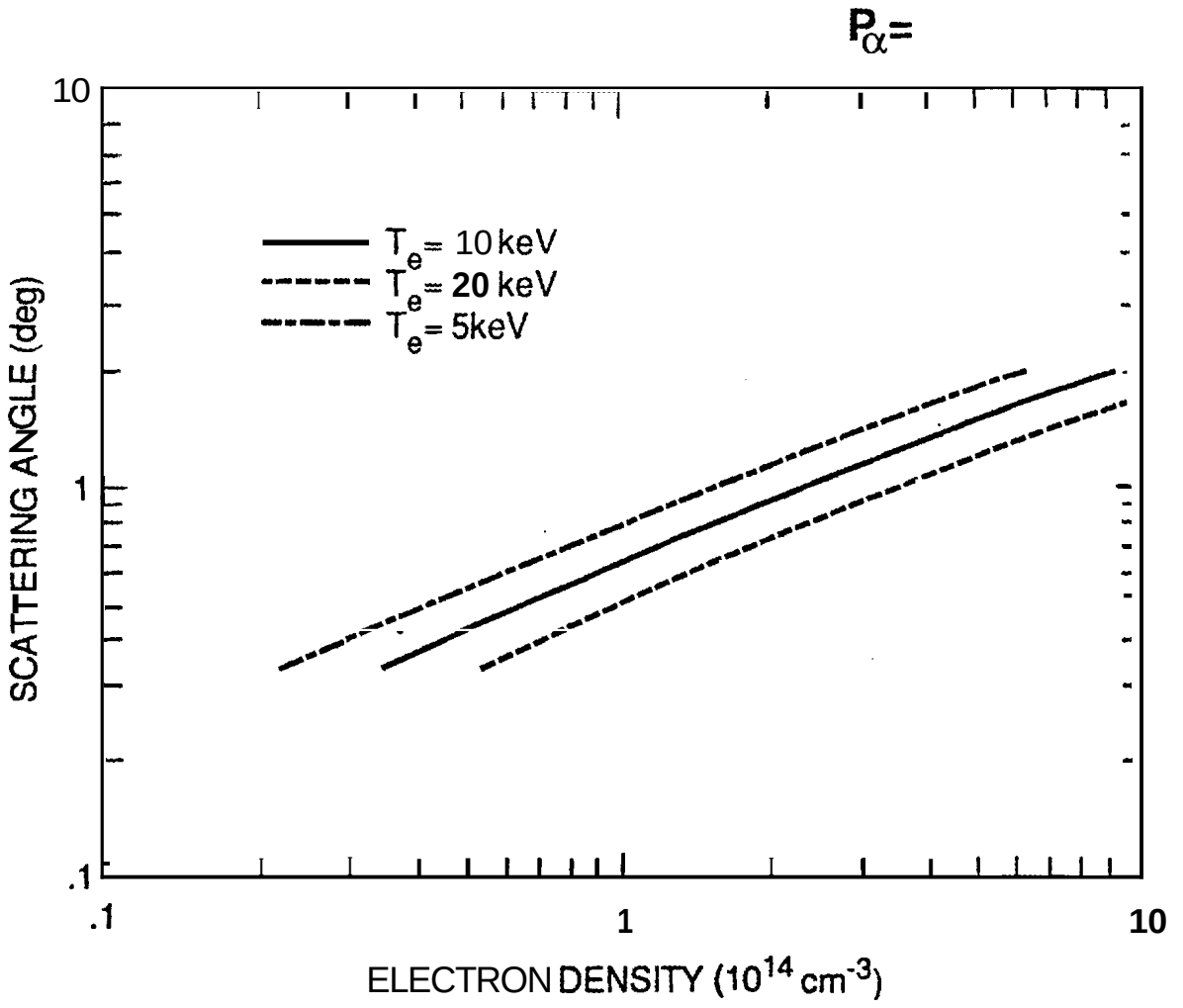

Fig. 9. The scattering angle for $P_\alpha = P_e$ versus electron density for a 20 cm scattering length, electron temperatures of 5, 10, and 20 keV; an alpha particle fraction of 1%, a 2 GHz receiver bandwidth, and the receiver frequency set by Eq. (11).

ORNL- DWG 92M-14319

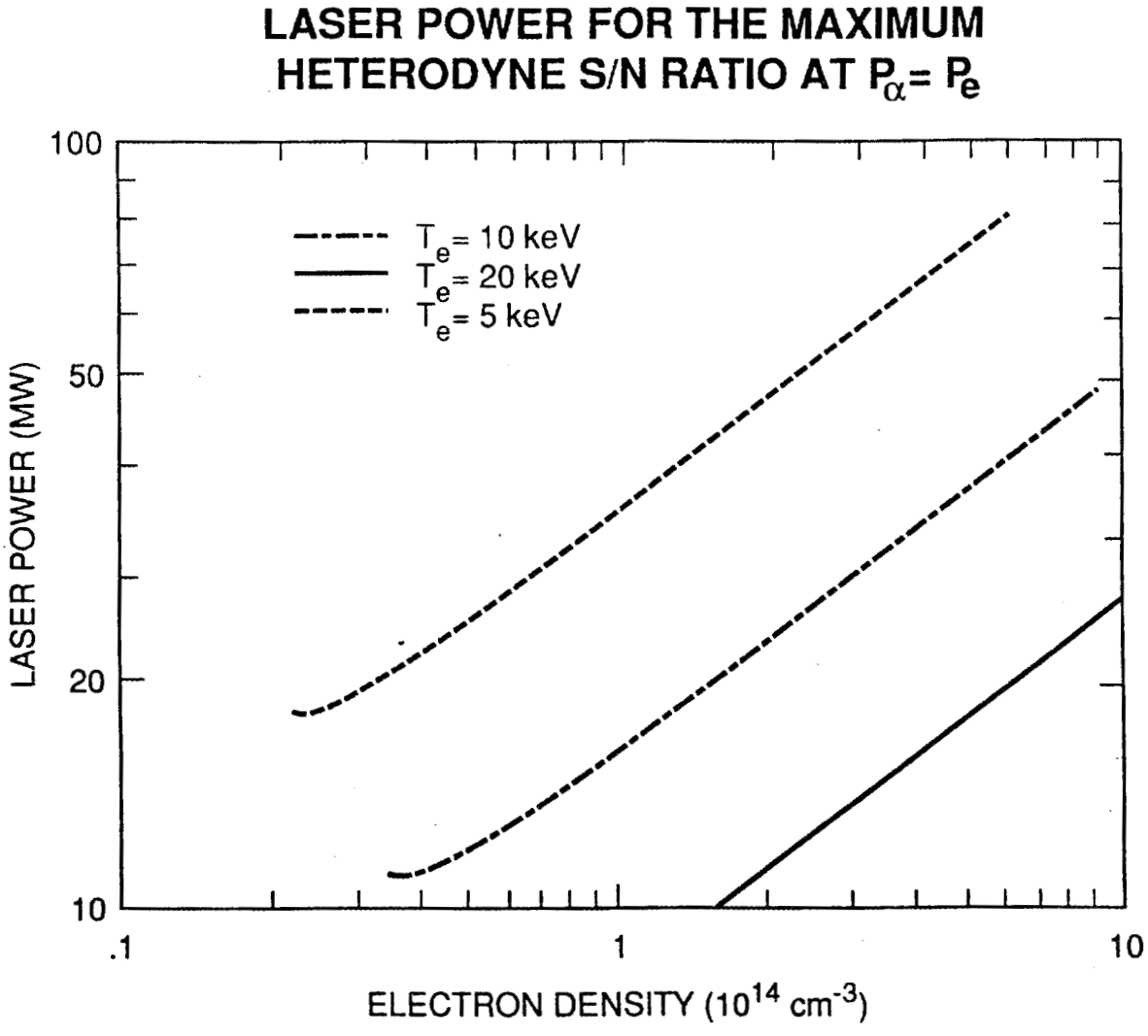

Fig. 10. The laser power which optimizes the signal-to-noise ratio for the conditions given in Fig. 9.

INTERNAL DISTRIBUTION

1. R. A. Dory
2-6. D. P. Hutchinson
7-11. C. H. Ma
12-16. R. K. Richards
17. J. Sheffield
18. Fusion Energy Division Library
19. Central Research Library
20. Document Reference Section
21-22. Laboratory Records
23. Laboratory Records, RC
24. ORNL Patent Section

EXTERNAL DISTRIBUTION

25. Office of the Assistant Manager for Energy Research and Development, Department of Energy, Oak Ridge Operations, Box 2008, Oak Ridge, TN 37831
26-27. Office of Scientific and Technical Information, P.O. Box 62, Oak Ridge, TN 37831
28. R. Aymar, CEN/Cadarache, Department de Recherches sur la Fusion Controlée, F-13108 Sain-Paul-lez-Durance, Cedex, France
29. C. A. Bennett, Dept. of Physics, Univ. of North Carolina-Asheville, Asheville, NC 28814
30. Bibliothek, Institut für Plasmaphysik, KFA Jülich GmbH, Postfach 1913, D-5170 Jülich, Federal Republic of Germany
31. Bibliothek, Max-Planck Institut für Plasmaphysik, Boltzmannstrasse 2, D-8046 Garching, Federal Republic of Germany
32. Bibliothek, KfK Karlsruhe GmbH, Postfach 3640, D-7500 Karlsruhe 1, Federal Republic of Germany
33. Bibliotheque, Centre de Recherches en Physique des Plasmas, Ecole Polytechnique Fédérale de Lausanne, 21 Avenue des Bains, CH-1007 Lausanne, Switzerland
34. Bibliothèque, CEN/Cadarache, F-13108 Saint-Paul-lez-Durance, Cedex, France
35. N. L. Bretz, Princeton Plasma Physics Laboratory, P.O. Box 451, Princeton, NJ 08544
36. J. D. Callen, Dept. of Nucl. Eng., Univ. of Wisconsin, Madison, WI 53706-1687
37. R. W. Conn, Dept. of Chemical, Nuclear, and Thermal Engineering, Univ. of California, Los Angeles, CA 90024
38. D. H. Crandall, ER-54 G-219/GTN, Office of Fusion Energy, U.S. Dept. of Energy, Washington, DC 20585
39. N. Anne Davies, Associate Director for Fusion Energy, Office of Energy Research, ER-50 Germantown, DOE, Washington, D.C. 20585
40. S. O. Dean, Fusion Power Associates, 2 Professional Dr., Suite 248, Gaithersburg, MD 20879
41. G. A. Eliseev, I. V. Kurchatov Inst. of Atomic Energy, P.O. Box 3402, 123182 Moscow, Russia
42. D. Evans, Culham Laboratory, Abingdon, Oxon. OX14 3DB, United Kingdom
43. M. Forrest, JET, Culham Laboratory, Abingdon, Oxon. OX14 3DB, United Kingdom
44. H. K. Forsen, Bechtel Group, Inc., Research Engineering, P.O. Box 3965, San Francisco, CA 94119

45. J. R. Gilleland, L-644, Lawrence Livermore National Laboratory, P.O. Box 5511, Livermore, CA 94550
46. V. A. Glukhikh, Scientific-Research Inst. of Electro-Physical Apparatus, 188631 Leningrad, Russia
47. R. W. Gould, Dept. of Applied Physics, California Inst. of Technology, Pasadena, CA 91125
48. C. Gowers, JET, Culham Laboratory, Abingdon, Oxon. OX14 3DB, United Kingdom
49. R. A. Gross, Plasma Research Lab., Columbia Univ., New York, NY 10027
50. Director, The Institute of Plasma Physics, P.O. Box 26, Hefei, Anhui, China (PRC)
51. F. C. Jahoda, Los Alamos Scientific Laboratory, University of California, P.O. Box 1663, Los Alamos, NM 87545
52. Library, Centro Richerche Energia Frascati, C.P. 65, I-00044 Frascati (Roma), Italy
53. Library, Culham Lab., UKAEA, Abingdon, Oxfordshire, OX14 3DB, England
54. Library, JET Joint Undertaking, Abingdon, Oxfordshire OX14 3EA, England
55. Library, FOM Inst. voor Plasmafysica, Rijnhuizen, Edisonbaan 14, 3439 NM Nieuwegein, The Netherlands
56. Library, National Inst. of Fusion Science, Nagoya Univ., Chikusa-ku, Nagoya 464-01, Japan
57. Library, International Center for Theoretical Physics, P.O. Box 586, I-34100 Trieste, Italy
58. Library, Plasma Physics Laboratory, Kyoto Univ., Gokasho, Uji, Kyoto 611, Japan
59. N. C. Luhmann, 7702 Boelter Hall, Electrical Engineering Dept., School of Engineering and Applied Science, 405 Hilgard Ave., Univ. of California, Los Angeles, CA 90024
60. D. Markevich, Office of Fusion Energy, Department of Energy, Washington, DC 20585
61. K. McCormick, Max-Planck Institut für Plasmaphysik, 8046 Garching bei Munchen, Germany
62. R. H. McKnight, Office of Fusion Energy, Department of Energy, Washington, DC 20585
63. D. M. Meade, Plasma Physics Lab., Princeton Univ., P.O. Box 451, Princeton, NJ 08544
64. O. Pavlichenko, Kharkov Physical-Technical Inst., Academical St. 1, 310108 Kharkov, Russia
65. R. R. Patty, Dept. of Physics, North Carolina State Univ., Raleigh, NC 27650
66. R. A. Phaneuf, Dept. of Physics/220, University of Nevada, Reno, NV 89557
67. Plasma Research Laboratory, Australian National Univ., P.O. Box 4, Canberra, A.C.T. 2601, Australia
68. M. Roberts, International Programs, Office of Fusion Energy, Office of Energy Research, ER-52 Germantown, Department of Energy, Washington, DC 20585
69. D. D. Ryutov, Inst. of Nuclear Physics, Siberian Branch, Academy of Sciences of Russia, Sovetskaya St. 5, 630090 Novosibirsk, Russia
70. I. Shpigel, Inst. of General Physics, Russian Academy of Sciences, Ulitsa Vavilova 38, Moscow, Russia
71. Deputy Director, Southwestern Institute of Physics, P.O. Box 15, Leshan, Sichuan, China (PRC)

72. W. M. Stacey, Jr., School of Nuclear Engineering, Georgia Inst. of Technology, Atlanta, GA 30332
73. D. Steiner, Nuclear Engineering Dept., NES Building, Tibbetts Avenue, Rensselaer Polytechnic Institute, Troy, NY 12181
74. J. D. Strachan, Princeton Plasma Physics Laboratory, P.O. Box 451, Princeton, NJ 08544
75. R. Varma, Physical Research Lab., Navrangpura, Ahmedabad 380009, India
76. M. Yamanaka, Dept. of Applied Physics, Osaka University, Yamada-kami, Suita, Osaka 565, Japan
77. K. M. Young, Princeton Plasma Physics Laboratory, P.O. Box 451, Princeton, NJ 08544
78. S. Zweben, Princeton Plasma Physics Laboratory, P.O. Box 451, Princeton, NJ 08544